The Journal of Experimental Biology 209, 1122-1134
Published by The Company of Biologists 2006
doi:10.1242/jeb.02080

The role of single spiking spherical neurons in a fast sensory pathway

Javier Nogueira[1,2], María E. Castelló[1,2] and Angel Ariel Caputi[1,*]

[1]*Department of Integrative and Computational Neurosciences, Instituto de Investigaciones Biológicas Clemente Estable, Associated Unit of the Facultad de Ciencias, Universidad de la República, Av. Italia 3318, Montevideo, Uruguay and* [2]*Department of Histology and Embriology, Facultad de Medicina, Universidad de la República, Gral. Flores 2515, Montevideo, Uruguay*

*Author for correspondence (e-mail: angel@iibce.edu.uy)

Accepted 5 January 2006

Summary

One difficulty in understanding the brain is that of linking the structure of the neurons with their computational roles in neural circuits. In this paper we address this subject in a relative simple system, the fast electrosensory pathway of an electric fish, where sensory images are coded by the relative latency of a volley of single spikes. The main input to this path is a stream of discrete electric images resulting from the modulation of a self-generated carrier by the environment. At the second order cell level, a window of low responsiveness, reducing potential interference from other stimuli, follows activation of the path.

In the present study, we further characterize the input–output relationship at the second order neurons by recording field potentials, and ascertain its cellular basis using *in vitro* whole cell patch recordings. The field potentials from freely behaving, socially interacting fish were obtained from chronically implanted fish restrained in a mesh pen. In addition, at the end of some experiments the fish was curarized and the fast electrosensory path responses to artificial stimuli were further explored. These *in vivo* approaches showed that larger stimuli cause larger and longer windows of low responsiveness. The simple spherical geometry of the second order cells allowed us to unveil the membrane mechanisms underlying this phenomenon *in vitro*. These spherical cells respond with a single spike at the onset of current steps of any amplitude and duration, showing inward and outward rectification, and a long refractory period. We postulate that a low-threshold K^+ conductance generates the outward rectification. The most parsimonious interpretation of our data indicates that slow deactivation of this conductance causes the long refractory period. These non-linear properties of the membrane explain the single spiking profile of spherical cells and the low-responsiveness window observed *in vivo*. Since the electric organ discharges are emitted at intervals slightly longer than the duration of the low-responsiveness window, we propose that the described cellular mechanisms allow fish streaming self-generated images.

Key words: intrinsic properties, electroreception, time coding, low-responsiveness window, onset neuron, electric fish.

Introduction

Understanding how neurons implement the computations required for the function of the neural networks in which they are inserted is a difficult task, because of the variety of neuron types and the complexity of the circuits that they form. Another difficulty is that neurons are characterized by their geometry, membrane electrogenic properties and intracellular regulatory processes, extending the concept of 'intrinsic properties' (Llinas, 1988), whereas the computations performed by circuits are characterized by the signals encoded and the relationship between input and output (Marr, 1982; Arbib et al., 1997). These difficulties are more easily overcome by studying neurons of simple geometry belonging to relatively simple circuits where the links between the structure of a neuron and its functional role in a network can be more readily established (Marder, 2002; Koch and Segev, 2000). This paper addresses this problem in spherically shaped cells belonging to a particularly simple circuit of a gymnotid electric fish of the pulse type.

Pulse gymnotids and other electric fish use their electric organ discharges (EOD) as a carrier for sensory signals (Lissmann, 1951; Lissmann, 1958; Aguilera et al., 2001). Objects in the fish's close environment modify the self-generated electric field causing object-related patterns of transcutaneous current density (electric images) that stimulate cutaneous electroreceptors (Bullock et al., 1961). Electrosensory signals are detected by electroreceptors innervated by afferent fibers projecting to the electrosensory lobe (ELL) of the medulla.

Afferents from one class of electroreceptors are known as

pulse markers. These afferents encode the amplitude of the local stimulus using the latency of a single spike. Pulse marker afferents terminate centrally on the cell bodies of spherical cells in the deeper layers of the ELL by way of morphologically mixed synapses (Castelló et al., 1998; Réthelyi and Szabo, 1973).

Spherical cells have few short dendrites that make gap junctions with the soma of neighboring spherical cells, and also receive chemical axosomatic or axodendritic contacts from thin fibers from still unknown origin (Castelló et al., 1998). Spherical cell axons project to the mesencephalic magnocellular nucleus by way of the lateral lemniscus. The pathway that comprises the pulse marker afferents, the ELL spherical cells and the mesencephalic magnocellular nucleus, is referred to as the fast electrosensory pathway (Szabo et al., 1975).

This paper focuses on the intrinsic properties and the computational role of ELL spherical cells.

We have previously implemented a methodology to record the activity of electrosensory structures *in vivo* in the freely moving fish (Castelló et al., 1998; Pereira et al., 2005). We found that the characteristic sign of the activation of the fast electrosensory pathway is a brief compound action potential occurring shortly after the self-generated or conspecific-generated EODs. These field potential recordings can be obtained all along the path; that is, in the electrosensory nerve (a sign of spherical cells afferent input), the ELL, the lateral lemniscus (a sign of the spherical cells output) and the magnocellular nucleus.

The input–output relationship of the spherical cell population has two main features: (i) synchronization and precise timing of spherical cells firing, and (ii) a low-responsiveness time window after the activation of the fast electrosensory pathway by the self-generated EOD that is slightly shorter in duration than the inter-EOD interval. The precise synchronism between spherical cells is revealed by the sharpness and phase locking of the lemniscal compound action potential, and by the strong correlation between the amplitude of primary afferent and lemniscal compound action potentials (Szabo et al., 1975; Castelló et al., 1998). The low-responsiveness window prevents the subsequent activation of the path by externally generated, potentially interfering signals (Schlegel, 1973; Castelló et al., 1998). This phenomenon appears to reflect a trade-off between electrolocation, in which responses to the EODs of other fish are a form of interference, and electro-communication, in which such EODs are the signals of interest (Westby, 1975; Capurro et al., 1998; Westby, 1979; Black Cleworth, 1969).

The present study addresses the question of how the intrinsic membrane properties of spherical cells determine the input–output relationship of the fast electrosensory pathway at the level of the ELL. Recordings were made both *in vivo* in the freely discharging fish and in slice preparations *in vitro*. We found that the length of the low-responsiveness window depends on the relative amplitude of self- and conspecific-generated EODs. We also found that voltage dependent conductances in spherical cells endow them with an onset spiking profile and a long refractory period that corresponds to the low-responsiveness window observed *in vivo*.

Materials and methods

General

All experiments were performed in fish of the genus *Gymnotus* ranging between 12 and 18 cm in length. This species is easily gathered in lakes and creeks close to Montevideo (latitude 35.5°, longitude 55°). The species was previously identified as *G. carapo*, but after extensive re-examination of the genus by Albert (Albert and Crampton, 2005), its identity remains uncertain. Fish care and experiments were performed under the regulations of the Comisión Honoraria de Experimentación Animal of the Universidad de la República (ordinance 4332-99) and the International Guiding Principles for Biomedical Research Involving Animals. All surgical procedures were performed under deep anesthesia induced by cold. For this purpose, the gills were perfused with aerated water at 4°C throughout the surgery. After a few minutes of cold-water perfusion, the EOD and the motor responses to nociceptive stimuli stop. Cold anesthesia is completely reversible if temperature transitions are performed slowly.

Field potential recordings in vivo

The activity evoked at the magnocellular mesencephalic nucleus by self- and conspecific-generated EODs, or artificial stimuli, was recorded using two attached wires (80 μm diameter, insulated except at their tips) lowered through a small hole in the skull down to 1000–1200 μm from the brain surface, and attached with dental cement. Signals were differentially amplified (gain ×1000), band-pass filtered (10–10 000 Hz), and digitized with an oscilloscope for on-line visual inspection and for off-line analysis.

In one group of experiments, the animals were first chronically implanted and then restrained in a narrow pen made of plastic screen. Freely discharging conspecifics were also restrained in a similar separated pen, located at different positions and distances from the recorded fish. The self- and conspecific-generated EODs were recorded. In some cases the conspecific EOD was mimicked by a 3 ms current 'square' pulse applied between two electrodes 10 cm apart, on a parallel line to the recorded fish, at a constant distance in each experiment.

In another group of experiments, the same kinds of recordings were obtained from curarized fish to study the effect of the amplitude of the conditioning and the test stimuli on the low-responsiveness window. In this case, conditioning stimuli consisted of current 'square' pulses (3 ms, 5–30 Hz) applied between a wire inserted in the dorsal muscle mass and a 1.5 cm stainless steel disc in front of the jaw (a region where the electrosensory fovea is located and the electroreceptors are most dense) by injecting current 'square' pulses (3 ms) between the wire in the muscle mass and an insulated wire

(100 μm diameter) with its bare tip facing the site where the maximal response at the magnocellularis nucleus was evoked with minimal intensity. This kind of stimulation allowed us to explore the response of the path to a local test stimulus delivered at the center of the receptive field of the recorded region. Conditioning and test steps were generated by two different, optically coupled and battery-operated stimulus isolation units. We examined the effects of three variables by changing one at a time: the intensity of the conditioning stimulus, the intensity of the test stimulus, and the delay between conditioning and test stimuli. Intensities of both stimuli were scaled by their respective thresholds, defined as the minimal current intensity that evoked a noticeable response in one half of the trials.

Intracellular recordings of spherical cells

Brain slices transverse to the main axis of the brain were obtained using a vibratome. Slices were incubated in a low sodium solution containing (mmol l^{-1}): KCl (2), $CaCl_2$ (2.6), $KHPO_4$ (1.25), $NaHCO_3$ (24), $MgSO_4$ (1.6), glucose (20), NaCl (0) and sucrose (201), pH 7.4. After a period of 30–60 min, slices were transferred to the standard recording solution of the same composition but lacking sucrose and having a physiological concentration of NaCl (120 mmol l^{-1}). Spherical cells are located at the border between the deep neuropil and granule cell layers of ELL and could be identified using Nomarski optics under infrared illumination. Whole cell patch recordings were obtained using 5–10 MΩ tip-polished microelectrodes filled with a solution containing the following (mmol l^{-1}): potassium gluconate 122, $MgCl_2$ 2.5, magnesium gluconate 5.6, $CaCl_2$ 0.3, Na_2ATP 5, K-Hepes 5, H-Hepes 5, EGTA 1 and biocytin 10, pH 7.4.

In current clamp conditions we studied cell membrane intrinsic properties by applying the following protocols: (i) in all cells, a series of steps differing in amplitude by a constant amount was repeated several times during the experiment; (ii) in 20 cells, paired pulsed stimulation using conditioning and test pulses of different amplitudes, delays and durations was used to explore cell excitability; and (iii) in four cells, series of steps, as described in (i), were applied at different delays after conditioning pulses, to determine the relationship between conductance changes and excitability. We used two parameters to evaluate excitability: spike latency and spike threshold. Spike latency was defined as the interval between the current step onset and the peak time of the spike. Spike threshold was defined as the minimum current intensity that evokes a spike for pulses of 20 ms or longer (spike latency was never longer than 3.5 ms). In addition, we studied the effects of steady currents manually applied while spikes were evoked with a brief intracellular stimulus. We analyzed the spike after-potential and also compared voltage *vs* current (*V/I*) plots obtained 1 ms before, 5 ms after and 10 ms after in order to determine the effect of a spike on current–voltage relationships. Cells were injected with biocytin after completion of intracellular protocols by passing depolarizing and hyperpolarizing alternating current steps.

After the experiment the tissue was fixed and biocytin in the recorded cells was revealed using a standard avidin–biotin–peroxidase–diaminobenzidine protocol (Horikawa and Armstrong, 1988).

Results

The input–output characteristics of the fast electrosensory pathway

Electric images projected on the skin cause compound action potentials at different levels of the fast electrosensory pathway corresponding to the synchronized activity of the afferent population (the ELL input), the spherical cell axons traveling along the lateral lemniscus (the ELL output), and the magnocellularis nucleus large cells (Castelló et al., 1998). In the absence of skin electrical stimuli the fast electrosensory pathway is silent.

The amplitude of the spherical cell axon's compound potential is linearly related to the amplitude of self-generated EOD (Pereira et al., 2005). However, the amplitude of the responses evoked by conspecifics depends strongly on the interval between the self-generated EOD and the conspecific-generated EOD. This interval decreases progressively when the conspecific EOD rate is slightly higher and increases progressively when it is slightly lower. In association with the decrease in interval between self- and conspecific-generated EODs there is also a reduction in amplitude of the conspecific-generated EOD-evoked responses recorded in the lateral lemniscus and magnocellularis nucleus, but there is no such amplitude reduction in evoked responses recorded in the mandibular nerve. This indicates that activation of the ELL structures of the fast electrosensory pathway by the self-generated EOD causes a low-responsiveness window (Castelló et al., 1998). This phenomenon is exemplified in Fig. 1, showing the effects of the fast electrosensory pathway activation by the self-generated EOD and the conspecific-generated EOD of a neighbor fish with a slightly higher EOD rate. Consecutive traces, starting few milliseconds before the self-generated EOD and lasting about one EOD cycle of the recorded fish, show its magnocellularis nucleus responses to five self-generated EODs (referred to as 1–5) and to seven conspecific-generated EODs (referred to as a–g, green). The largest responses are caused by the self-generated EOD. The first trace illustrates the decrease in responsiveness after the self-generated EOD: while the second conspecific-generated EOD occurring at longer delay (conspecific-generated EODb) causes a large response, the first one, occurring shortly after the self-generated EOD (conspecific-generated EODa), does not cause any response. The temporal profile of the low-responsiveness window is shown in traces 2–4 in which the interval between the self-generated EOD and the conspecific-generated EOD decreases progressively and the response to the conspecific-generated EOD is gradually reduced. The last trace 5, marks f and g, shows a return to the beginning of the sweeping cycle caused by the small difference in EOD rate. Note that, consistent with previous findings (Castelló et al.,

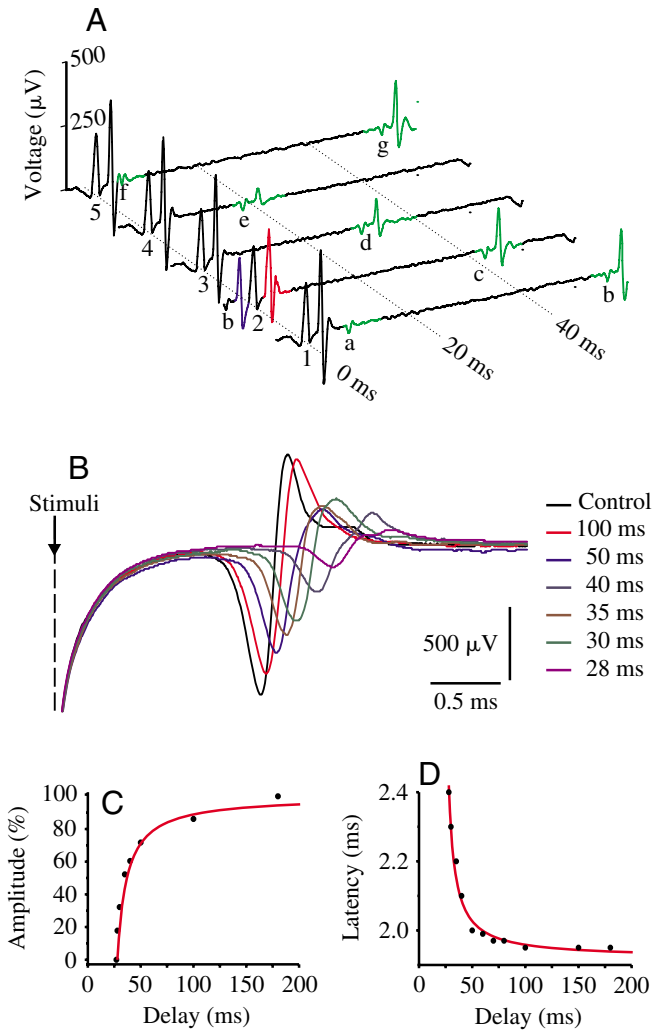

Fig. 1. The low-responsiveness window of the fast electrosensory pathway is elicited by natural (A) and artificial (B–D) stimuli. (A) Field potentials evoked by the self- (black triphasic artifact around time zero in each trace) and conspecific (green)-generated EODs at the magnocellularis nucleus in a freely moving fish. The triphasic waveform at the beginning of each trace (labeled 1–5) is the sEOD artifact, followed by a spike corresponding to the fast electrosensory pathway evoked response. The cEOD artifact is the small triphasic waveform highlighted in green (labeled a–g). The fast electrosensory pathway response evoked by the conspecific-generated EOD (green spikes) is absent at short delays (a and f) and increases in amplitude with the interval between the self-generated EOD and the conspecific-generated EOD (green evoked spikes labeled e, d, c and b). Note that a similar, but smaller, decrease in the response to the self-generated EOD is provoked by the activation of the fast electrosensory pathway when the conspecific-generated EOD (second trace, blue spike) occurs just before the self-generated EOD (red spike). (B) Field potential responses evoked in the magnocellularis nucleus of a curarized fish by a two-threshold artificial stimulus delivered at different periods (28–100 ms) after a conditioning stimulus (evoking a response similar to that evoked by the self-generated EOD). With short delays after the activation of the fast electrosensory pathway responsiveness is reduced, as indicated by a decrease in amplitude (C) and an increase in latency (D) of the response elicited by the artificial test stimulus.

1998), the phenomenon is triggered by the activation of the fast electrosensory pathway, since the low-responsiveness window is also elicited by the conspecific-generated EOD (conspecific-generated EODb in blue) when it closely precedes the self-generated EOD 2 (red).

To further study the characteristics of the low-responsiveness window, we used similar recordings in a curarized preparation. To mimic the fish's own EOD we delivered a conditioning current pulse to the jaw (a region where the electrosensory fovea is located and electroreceptors are most dense) and a test current pulse, locally stimulating a small site of the skin with a thin electrode (a 100 μm insulated wire except at the tip) at the center of the receptive field (see Materials and methods).

In the first set of experiments with curarized fish, we adjusted and maintained constant the conditioning stimulus intensity to match the response evoked by the self-generated EOD recorded in the same fish before curare. Responses evoked by the test stimulus increased in amplitude and decreased in latency as the delay between the conditioning and test pulses increased (Fig. 1B–D). Larger test stimuli generated larger responses when they were delivered after the same delay (Fig. 2A). Similarly, larger stimuli, such as those produced by a nearby conspecific, more easily overcame the low-responsiveness window than smaller stimuli elicited by the same conspecific at a longer distance (Fig. 2B,C).

In a second set of experiments with curarized fish, we studied the effect of conditioning stimulus intensity on the response to test stimuli of constant intensity (twice the intensity value at threshold) applied at different delays. The amplitude of the averaged response at each delay decreased as the intensity of the conditioning stimulus increased, shifting to the right the curves relating the amplitude of the response with the delay between the conditioning and test pulses (Fig. 3).

Cellular basis of the fast electrosensory pathway's input–output relationship

As mentioned above, previous results indicate that the low-responsiveness window is produced at the spherical cell level (Castelló et al., 1998). To elucidate the cellular basis of this phenomenon we performed *in vitro* recordings from 24 spherical cells obtained from brain slices of 18 fish. Cells were identified by their shape and location between the deep neuropil layer and the granule cell layer, as observed with Nomarski optics under infrared illumination. These cells were silent at rest and showed median resting membrane potentials of –70.5 mV (range –61.2 to –74.2 mV) with low noise (coefficient of variation between 7×10^{-4} and 9×10^{-3}). Biocytin labeling confirmed the cell morphology in 6 of the 24 recorded neurons. Both somata and axon were completely filled in three cells (Fig. 4A).

Constant current steps surpassing a median critical depolarization level of –40 mV (range –48 to –34.3 mV, N=24) evoked only a single overshooting spike, regardless of stimulus duration or amplitude (Fig. 4B). The spike was characterized by a fast rising phase, a slower falling phase, and a post-spike

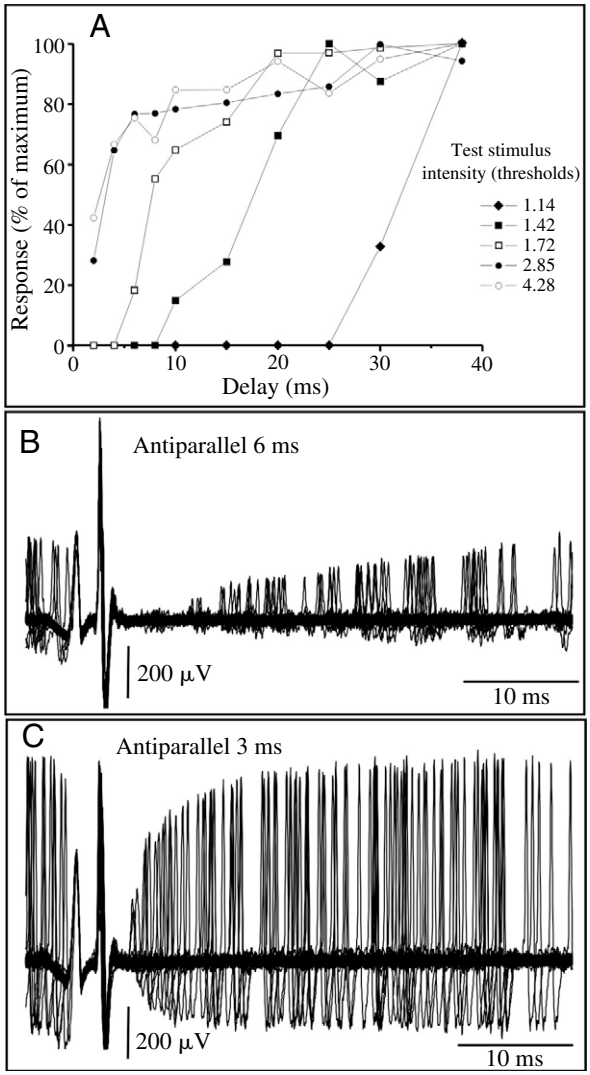

Fig. 2. The increase of the magnocellularis response with the intensity of the test stimuli or the conspecific-generated EOD shows that the low-responsiveness window is not an all-or-none phenomenon. (A) Amplitude of the magnocellularis nucleus responses to artificial test stimuli of different intensities as a function of the delay between the self-generated EOD and the test stimuli. The responses are expressed as a percentage of the maximal response evoked by the self-generated EOD. (B,C) Superimposed traces triggered by the self-generated EOD obtained in a fish chronically implanted in the magnocellularis nucleus, showing several responses evoked by the conspecific-generated EOD of a fish of similar length (13 cm) placed antiparallel (B) 6 cm and (C) 3 cm away.

hyperpolarizing phase that was abolished if membrane potential was lowered below –80 mV (median value, *N*=4) by passing a steady current. The latency of the spike decreased with stimulus intensity (Fig. 4B–D). In 4 out of 24 cells, the spike arose on the falling phase of a current-evoked hump (Fig. 4C, black and red traces), suggesting that the spike is initiated at an electrically distant site, probably at the axon.

Equal amounts of subthreshold depolarizing and hyperpolarizing current injection had asymmetrical effects on

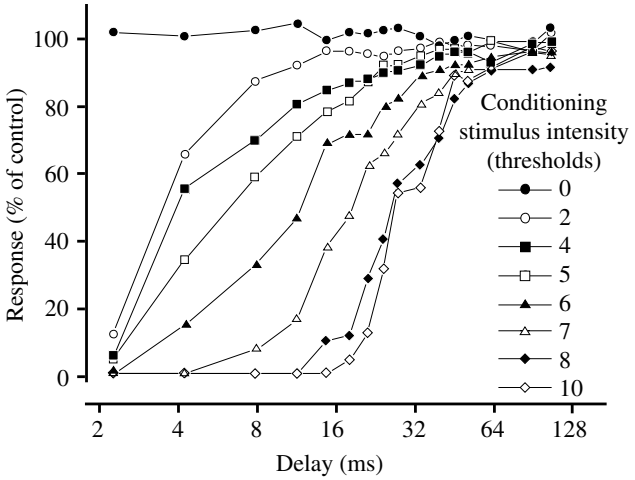

Fig. 3. The responsiveness of the fast electrosensory pathway decreases with the intensity of the conditioning stimuli. To assess the effect of activation of the fast electrosensory pathway on its responsiveness, the amplitude of the response of the magnocellularis nucleus to an artificial test stimulus of intensity 2× the threshold was studied as a function of the amplitude of an artificial conditioning stimulus, and the delay between conditioning and test stimuli, in a curarized fish. The amplitude of the test response (as a percentage of its maximal response) is plotted as a function of the delay between conditioning and test stimuli for eight conditioning stimulus intensities (0–10× threshold).

membrane potential, as shown by the time course of the voltage change during a long-lasting constant current pulse (up to 500 ms; Figs 5 and 6). The earlier changes in transmembrane voltage caused by current steps of different amplitude are analyzed in Fig. 5.

Subthreshold current steps depolarizing the cell above –65 mV (median, *N*=24) elicited a graded 'hump', peaking between 1.9 and 2.6 ms after the pulse onset. After the hump, membrane potential remained clamped at an even value depending on the amplitude of the current step (Fig. 5A,B). In addition, the hyperpolarization caused by current steps follows a non-exponential course, as shown by the deviation of the data points from a straight line in the semilogarithmic plot of voltage time derivative *vs* time (Fig. 5C). Consistently, this deviation was in the upper direction, indicating a progressive increase of the membrane impedance with hyperpolarization between 2 and about 10 ms.

Voltage *vs* current plots (*V*/*I* plots) constructed for a set of responses at different delays from the pulse onset allowed us to elucidate the mechanisms underlying this hump. The departure of the membrane potential from its resting value and the amplitude of the current step were proportional up to the peak of the hump occurring 2.4 ms after the onset (Fig. 5B, red line, 5D, red symbols), indicating that the rising phase is mainly consequence of the passive depolarization of the membrane by the injected current. The *V*/*I* plots after the peak of the hump were well fitted by a convex curve with two different limiting slopes for depolarizing and hyperpolarizing currents. Blue symbols in Fig. 5D exemplify this relationship

at 10.4 ms after the step onset (Fig. 5B, blue line, 5D, blue circles). While the hyperpolarizing limiting slope increased up to a maximum (Fig. 5D, solid line), the depolarizing limiting slope (Fig. 5D, dotted line) remained similar from the end of the hump up to the end of the steps (Fig. 5D, blue and green symbols). The depolarizing slope was on average 6–12 times smaller than the maximum slope for hyperpolarizing currents.

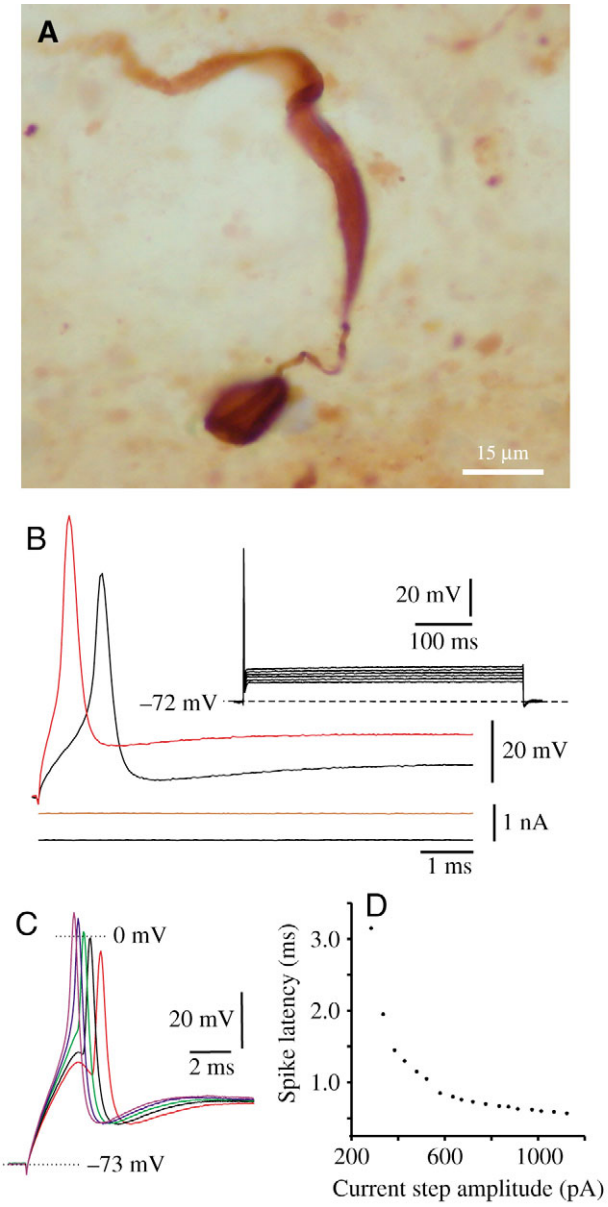

Fig. 4. The spherical cells 'phenotype'. (A,B) Biocytin-filled spherical cell characteristically firing a single spike when stimulated by long-lasting current step. (A) The spherical cells bear round smooth soma of about 15 µm diameter from which only one thin dendrite might emerge (not in this case) and a thick axon with a thin initial segment. (B) Traces from the same cell are displayed at a different magnification to show the shapes of the spikes (red and black traces) and the absence of repetitive firing with long lasting stimuli (inset). (C) Some cells (black and red traces) fire the spike on the falling face of a hump evoked by the stimulus step (stimuli in nA: violet 0.95; blue 0.75, green 0.60, black 0.50, red 0.40). (D) Spike latency was a hyperbolic function of the stimulus intensity (data from another cell).

This asymmetric deviation from proportionality after the peak of the hump implies that depolarizations above –65 mV trigger large and persistent increases in the equivalent membrane conductance without major changes in the negative equivalent electromotive force. It also suggests that a low-threshold outward current is the main cause of the hump-and-hold profile. Conductance reduction with hyperpolarization suggests that this conductance is partially active at rest.

The other important feature in the voltage profile evoked by constant current pulses was a depolarizing sag, starting 20–70 ms after the onset of hyperpolarizing steps in most cells (Figs 5A and 6A, black arrows). The hyperpolarizing limiting slope was maximal at the voltage peak just before the sag depolarization (median: 210 mV/pA; Figs 5D, 6D, green symbols). Consistent with the sag depolarization, the hyperpolarizing limiting slope just before the offset (Fig. 6A, red line, 6D, red symbols) decayed to an intermediate value between the maximal depolarizing (Fig. 6D, dotted line) and hyperpolarizing limiting slopes (Fig. 6D, continuous line).

These long-term changes in membrane conductance caused by the departure of the membrane potential from its resting value are also evident by comparing the voltage return to the resting potential after the offset of 50 and 200 ms current steps (Fig. 6A,B). Return curves after hyperpolarizations decayed much more slowly than after depolarizations. In addition, when the pulse was turned off at the peak of the hyperpolarization (Fig. 6B), the decay time (measured as the time where the voltage returned to half of the voltage departure from resting) was more than twice the value than for longer pulses in which the sag reached a plateau (Fig. 6A). While 50 ms hyperpolarization steps were followed by slow relaxation after the offset, longer hyperpolarizations causing large sag depolarizations were followed in half of the cells by 'rebound potentials' peaking about 20–25 ms after current offset (Figs 5A, asterisk, 6C). This suggests that the sag is due to a mixed-cation I_h conductance, and the rebound is the consequence of its remnant activation.

The excitability of the cell was systematically explored using paired intracellular pulses (conditioning and test steps) of different intensity, separated by different delays. These experiments demonstrated a long relative refractory period lasting from 10 to 40 ms, depending on the cell (Fig. 7A). The hump of the subthreshold response to the test step increased with the delay between pulses, but the depolarization after the hump remained similar (Fig. 7A). For a given delay and conditioning stimulus intensity, an increase in the intensity of the test stimulus provoked an increase in spike probability (Fig. 7A) and a reduction in spike latency (Fig. 7B). In addition, the latency of the spike evoked by the test pulse decreased with the delay between pulses (Fig. 7C). In all of 10 cells tested, a brief hyperpolarizing pulse after the conditioning stimulus suppressed these changes in excitability.

In order to correlate the observed effects on excitability with the changes in membrane conductance, *V*/*I* plots were

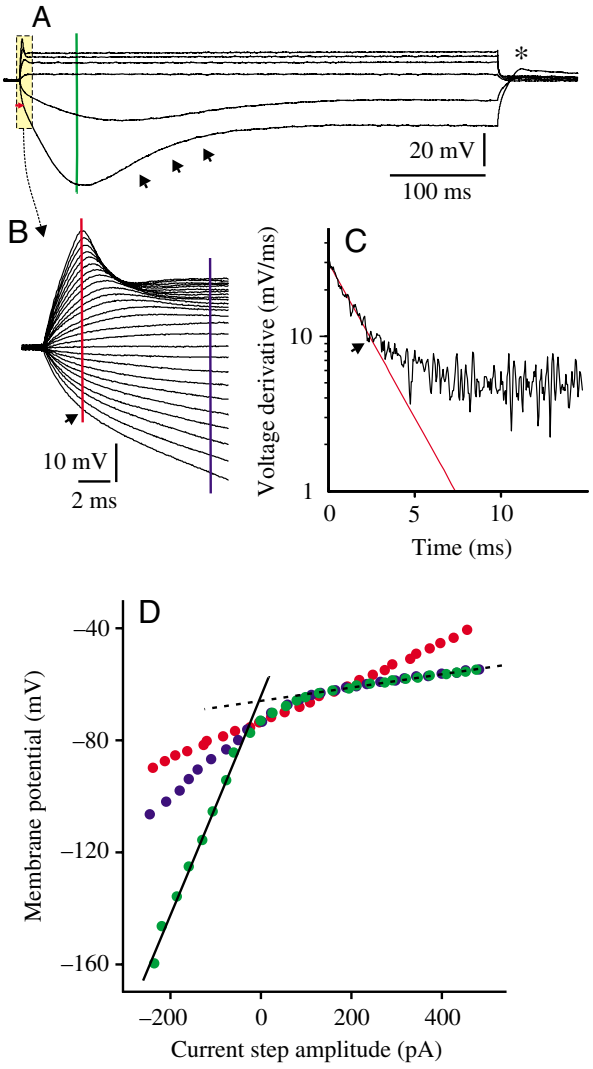

Fig. 5. Typical early subthreshold responses in a spherical cell. (A) Depolarizing and hyperpolarizing stimuli provoke very asymmetric responses. Note the hump-and-hold profile for depolarizing steps and a sag depolarization after 63 ms for hyperpolarizing steps (arrows in A, further analyzed in Fig. 6). (B) Enlarged version of the first 11 ms of the responses (boxed yellow in A, showing a hump peaking 2.4 ms after the stimulus onset (current steps are equally spaced by 25 pA). Up to this peak (red line in B) there is a linear relationship between membrane potential and injected current (red symbols in D). After this moment the response is asymmetric. For depolarizing steps there is a reduction of the voltage drop caused by the flow of injected current across the membrane and consequently an increase in membrane conductance. As shown by the coincidence of the depolarizing limiting slopes (broken line in D) of the *V/I* plots constructed for 10.4 ms (blue line in B; blue symbols in D) and 63 ms (green line in A; green symbols in D), there are no further changes in the *V/I* slope, indicating that the activated conductance does not inactive with time. For hyperpolarizing steps the semilogarithmic plot (C) of the voltage derivative *vs* time of the bottom voltage trace of B illustrates that there is a simple exponential relationship (red line) up to 2.4 ms (arrows in B,C). Beyond this time there is an upward departure from a simple exponential curve, indicating a reduction of membrane conductance.

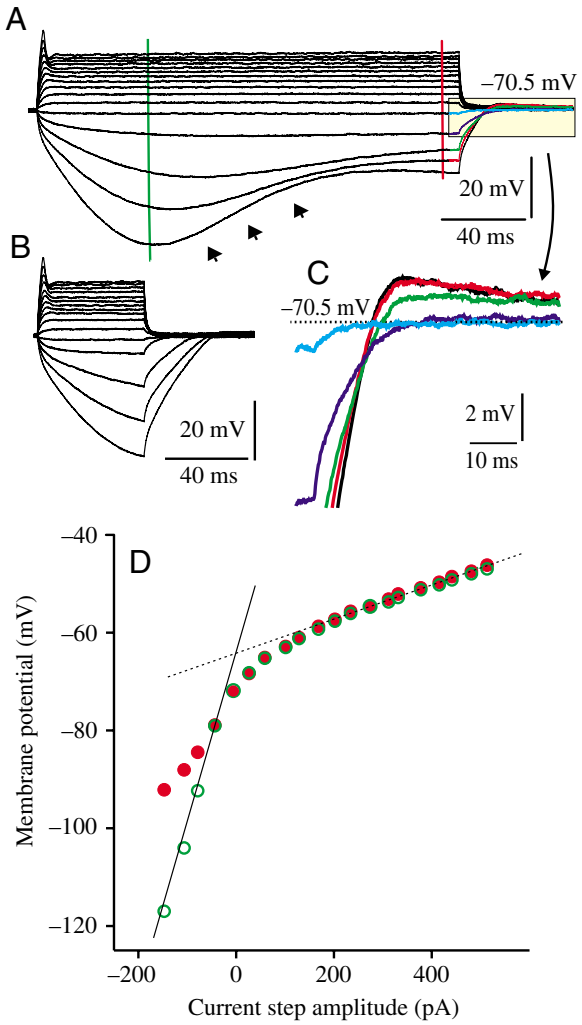

Fig. 6. Late responses to subthreshold pulses. Responses obtained from another cell to current steps of (A) 200 ms and (B) 50 ms. Current steps are equally spaced by 33 pA. For depolarizing currents, the long-lasting steps provoke an outward rectification, indicated by the reduction of the spacing between voltage recordings after the hump (A,B) and also by the comparing the *V/I* relationship obtained at 54 ms (green line in A) and 195 ms (red line in A) corresponding to red and green symbols fitted by the dotted line in D. For hyperpolarizing steps, beyond 54 ms after the onset (green line in A) there is an inward rectification with a sag depolarization (arrows in A), suggesting an increase of membrane conductance. Consequently, at the peak of the hyperpolarization the limiting slope for hyperpolarizing currents is maximal (green symbols fitted by the continuous line in D). At the end of the current step, the return curves for depolarizations have a much faster decay than for hyperpolarizations. When the hyperpolarizing current steps are ended at 50 ms (B), the return curve last much longer than when steps are ended at 200 ms (A). This matches the drop in the limiting slope of the hyperpolarizing side of the *V/I* plot (compare the continuous line and red circles in D). After the long pulse, there is a rebound graded with the amount of hyperpolarization as shown in C (enlarged version of the yellow shaded area in A).

constructed from the subthreshold responses of three cells to a series of intracellular current test pulses of different amplitude applied at different delays after a conditioning spike. The *V/I* plots 1 ms after the onset of the test step were always linear; thus, its slope can be considered as an indicator of the remnant change in membrane impedance caused by the conditioning pulse. Even though the slope measured at these short delays does not reveal the true membrane conductance (because current is also flowing through the cell's capacitance at this time), the changes in slope observed when applying test steps series at different delays are good indicators of the time course of the membrane conductance. The slope was smallest when the test step series was close to the conditioning stimulus offset, and it returned to basal values with the increase in delay between conditioning and test steps (Fig. 8A). In addition, the decrease in the V/I plot slope caused by decreasing the delay was well correlated with the increase in both the spike threshold (Fig. 8B) and the spike latency (Fig. 8C).

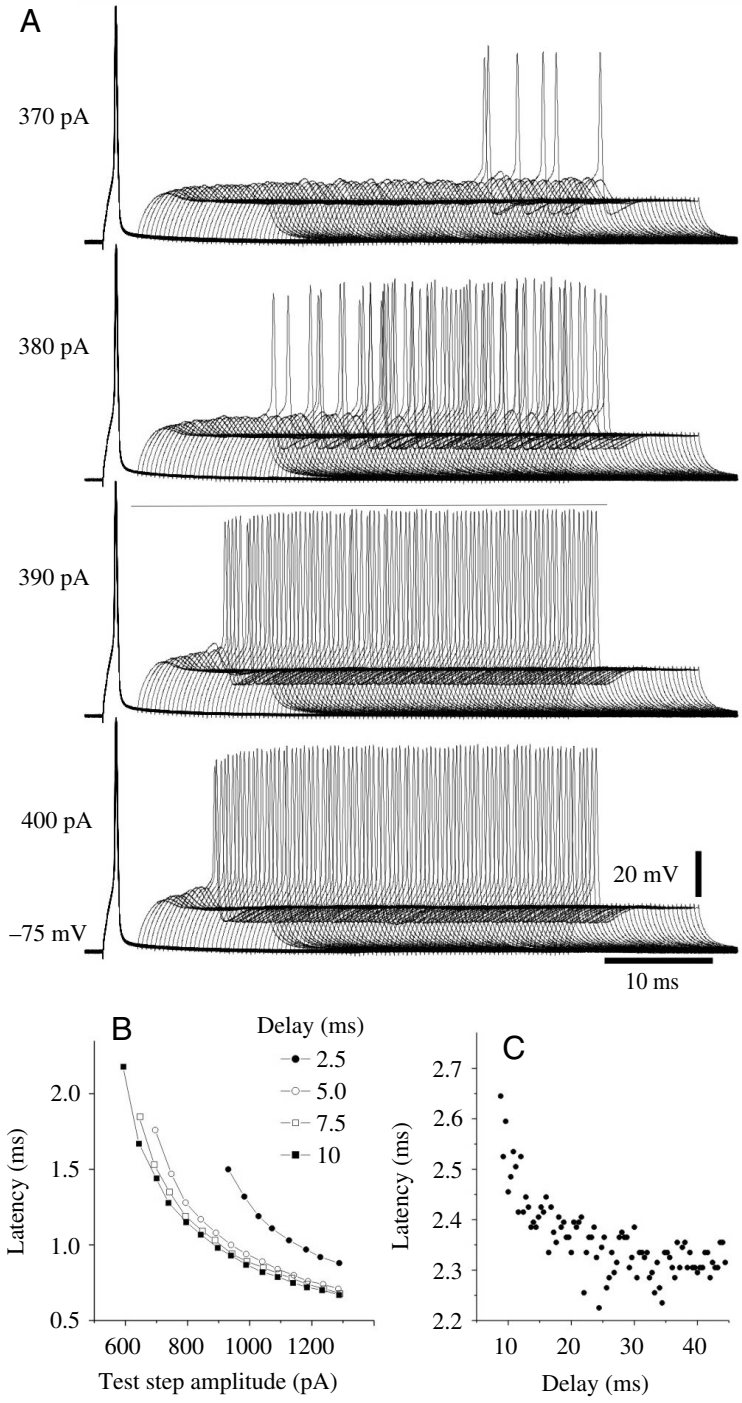

Fig. 7. Spherical cells have a long refractory period. Systematic stimulation of the cell with pairs of intracellular steps shows that the threshold and latency of the second spike depends on the delay between pulses. (A) Superimposed traces obtained stimulating with four different test step intensities (370, 380, 390 and 400 pA) at different delays from a conditioning step (800 pA). (B) Spike latency *vs* amplitude of the test step plotted for four different delays after a conditioning spike (data from another cell). (C) Spike latency *vs* delay plot corresponding to the experiment represented at the bottom row in A.

Interestingly, the spike was not necessary to provoke a decrease in excitability. Subthreshold conditioning depolarizations also caused a decrease in excitability that was graded with its amplitude (Fig. 9A, rows ii and iii). Furthermore, the amplitude of subthreshold responses to a test step was inversely related to the amplitude of a preceding subthreshold conditioning step (Fig. 9B). Therefore the conductances responsible for the changes in excitability are activated gradually by subthreshold depolarizations. In addition, after a depolarizing step the membrane potential showed an undershoot that was also graded with the step amplitude, confirming that the refractoriness is caused by a depolarization activated low-threshold outward conductance, which equilibrium potential is below the resting potential (Fig. 9B, arrows).

In two other cells the membrane potential was slowly changed while the spike was evoked at a normal EOD rate (25 Hz). This procedure showed a similar post-spike change in membrane conductance lasting between 10 and 15 ms (Fig. 10A). Accordingly, the slope of *V/I* plots obtained 5 and 10 ms (Fig. 10B, gray and black circles, respectively) after the spike were similar to the limiting depolarization slope and several times smaller than the slope obtained 1 ms before the spike (Fig. 10B, open circles).

Finally, *in vitro* results were compared with those obtained *in vivo*. The envelope of the averaged responses obtained using the paired pulse protocol described above and the plot of the amplitude of the field potentials as a function of the delay between self-generated EOD and conspecific-generated EOD showed a striking similarity (Fig. 11).

Discussion

Our results indicate that action potentials and subthreshold steps cause a long-lasting increase in membrane conductance that reduces neuron excitability,

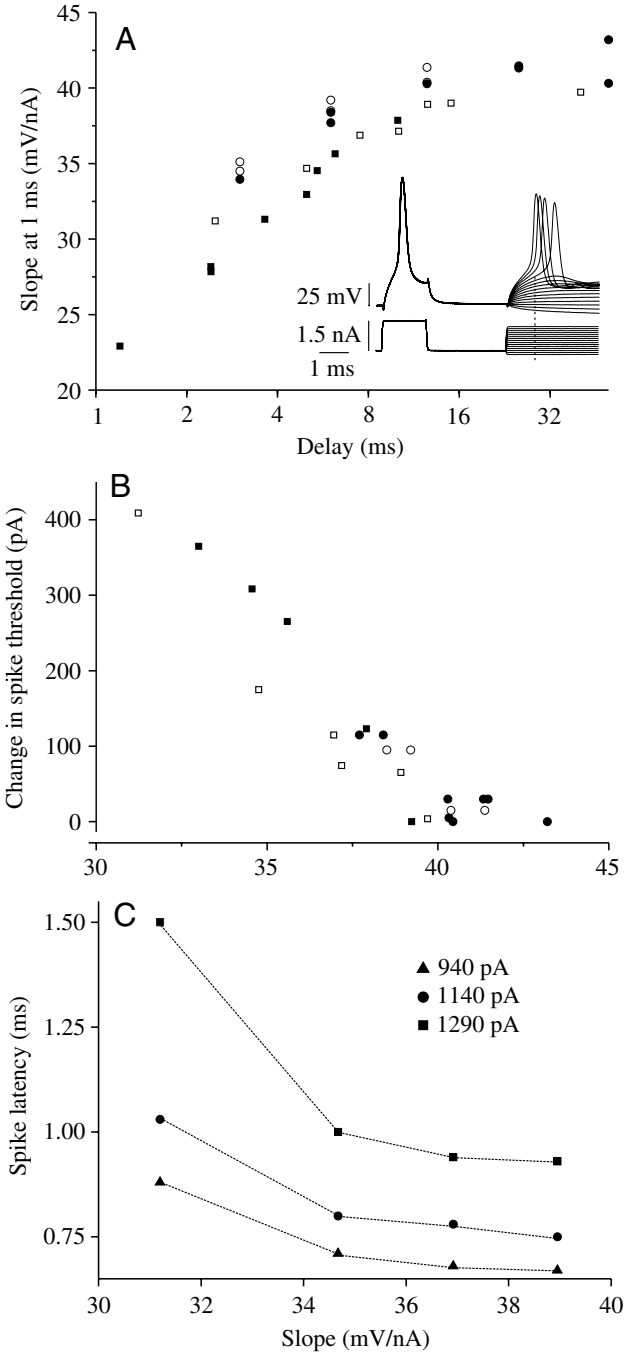

Fig. 8. Membrane conductance and the excitability of the cell change concomitantly after a conditioning spike. The change in membrane resistance was evaluated by the slope of the *V/I* plot constructed with data obtained 1 ms after the onset of a series of test current steps of different intensity (dotted line in inset) applied at different delays after a conditioning spike in four cells (symbol coded). (A) The increase in slope as a function of the delay indicates that after the conditioning spike there is an increase in membrane conductance and a slow return to resting values. (B,C) Change in spike threshold and spike latency as a function of the slope. Change in threshold was defined as the difference between the current intensity required for eliciting a spike when the stimulus was preceded by a conditioning spike at the given delay minus the current intensity required for eliciting a spike without a conditioning spike. As the spike threshold and latency decrease with the slope, the excitability of the cell is reduced by the increase of membrane conductance caused by the conditioning spike.

endowing spherical cells with the profile of a single spiking onset cell. They also suggest that the slow decay of a low-threshold outward rectifying K^+ conductance may subserve the long refractory period of spherical cells. This cellular phenomenon probably subserves the low-responsiveness window observed *in vivo* and its described properties.

ELL spherical cells are onset cells

Spherical cells, the secondary neurons of the fast electrosensory pathway, characteristically respond with a single spike to sustained steps. This is a common feature of so-called 'onset cells', a highly specialized neuronal type structurally adapted to transmit information using a latency code (Carr et al., 2005). As shown in Fig. 4C, the spike frequently arises from the falling phase of a hump, indicating that the recording site is not the lowest threshold site for the spike. Taking into account the spherical nature of the cell and its relatively small diameter, one may conclude that all the somata has similar membrane potential and that the spike initiates at the axon. Increases in cell conductance might drain synaptic currents, preventing generation of action potentials. Our results suggest that these attributes are conferred by the non-linear intrinsic membrane properties of the cell somata.

The outward rectification and the post-step undershoot graded with step amplitude (Fig. 8B arrows) indicate the activation of a low-threshold conductance having its equilibrium potential below the resting level, which could be either a K^+ or a Cl^- conductance. The activation of this low-threshold conductance shortly after the onset of small depolarizations explains the initial hump in the voltage recording. Voltage steadiness after this hump, and the constancy of the depolarizing limiting slope of the *V/I* curve, even for long-lasting depolarizations, indicates that the low-threshold conductance does not inactivate with time. The *V/I* curves obtained at the end of a series of long-lasting constant current steps showed large differences between depolarizing and hyperpolarizing limiting slopes, indicating that when low-threshold conductance is fully active, cell conductance is several times larger than at rest. However, the increase in membrane time constant 2.5 ms after the onset of an hyperpolarizing step suggests that the low-threshold conductance is partially active at rest (Fig. 5C). Outward rectification near the resting potential shortens the membrane time constant, and thus increases spike timing precision.

Preliminary data indicate that the low-threshold fast-activated and non-inactivating conductance is insensitive to tetraethylammonium (data not shown). This suggests that the conductance endowing the onset cell profile to spherical cells is similar to the K_{LT} described in the pyramidal cells of wave gymnotids (Fernández et al., 2005) and onset-neurons of other fast pathways (Carr et al., 2005).

Another characteristic that many ELL spherical cells share

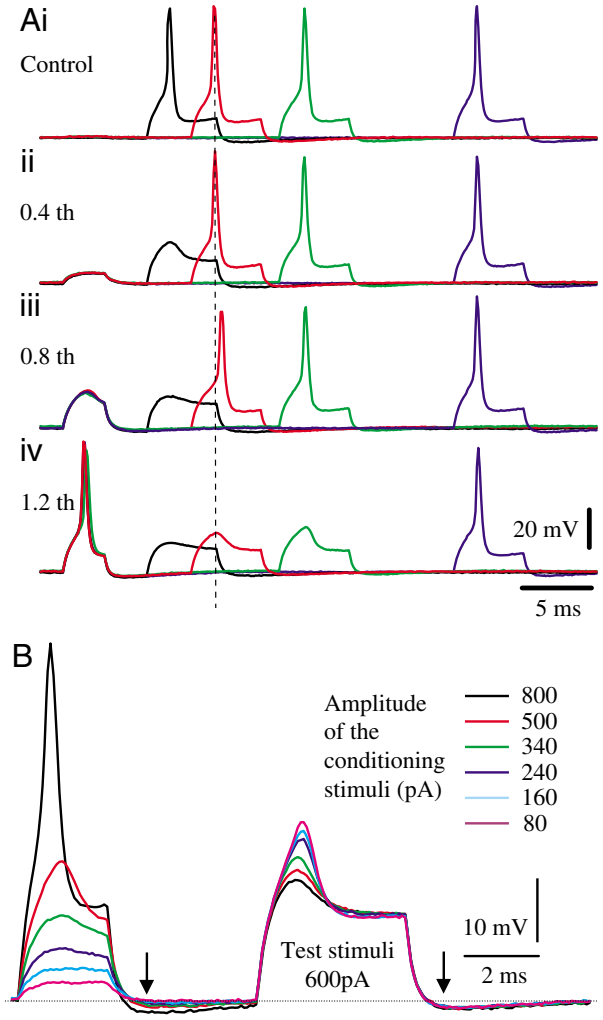

Fig. 9. Refractoriness is graded with the conditioning step intensity. (A) Responses evoked by four intracellular test steps (600 pA, 5 ms) applied at four different delays after 3 ms conditioning square steps of four different amplitudes 0, 200, 400 and 600 pA (i–iv, respectively). The increase in conditioning step amplitude cause: (a) depression of the hump in the subthreshold responses (compare black traces); (b) increase in spike latency (compare red spikes with the reference line); and (c) increase in spike threshold (lack of spikes in black traces in all rows except the control, red and green traces in row iv). (B) The amplitude of the hump evoked by a constant test stimulus (600 pA, 5 ms) decreases as the amplitude of the response evoked by the conditioning stimulus increases (color-coded, 3 ms). The maximum effect is caused when a conditioning spike is evoked. Note the undershoot after the sub-threshold stimuli (arrows).

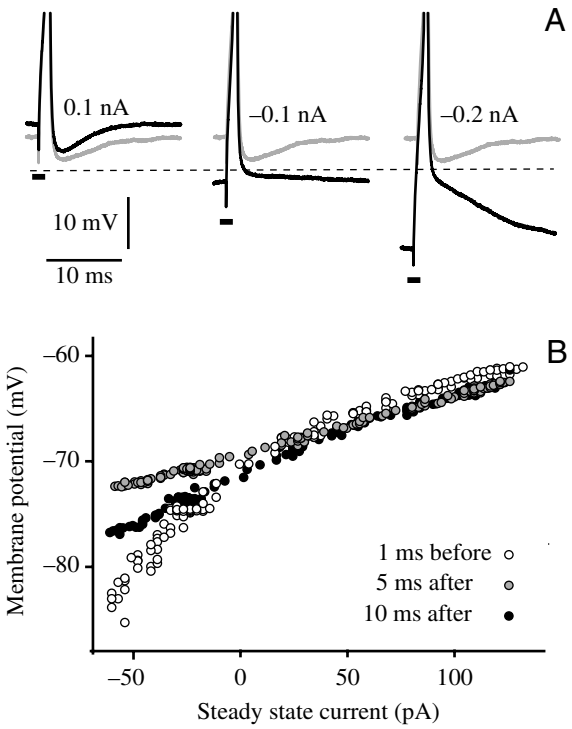

Fig. 10. Post-spike increase in membrane conductance as revealed by passing steady current. (A) Single spikes evoked by a brief pulse (bars) while passing different intensities of steady current (black traces). Superimposed gray traces correspond to control spikes without passing current. Note the inversion of the after-hyperpolarization when the basal membrane potential surpassed –80 mV (horizontal broken line). (B) *V/I* plots obtained in another cell, before (open symbols), 5 ms after (gray symbols) and 10 ms after the spike (black symbols). The linear relationship 5 ms after the spike (gray symbols) indicates that the spike causes an increase in conductance similar to that caused by the tonic depolarization of the membrane 1 ms before the spike (open symbols).

with other onset cells is their response to hyperpolarizing steps, with a depolarizing sag of the membrane potential starting between 20 and 70 ms after the step onset. The *V/I* slope at the end of a long-lasting step and the rate of voltage decay at its offset are less than half of those obtained with short-lasting (up to the peak of the hyperpolarization) current steps. This, and the rebound observed after the sag, indicate the presence of an inwardly rectifying, slowly activating and deactivating, mixed cation conductance. This family of conductances, referred to as I_Q or I_h, is present in many other preparations including some avian and mammalian auditory cells (Bal and Oertel, 2000; Trussell, 1999).

To sum up: we propose that the two main conductances defining the intrinsic properties of spherical cells are a low-threshold K^+ conductance and a mixed-cation hyperpolarizing activated conductance. Nevertheless, we cannot rule out the role of other conductances perhaps shaping spherical cell sub-phenotypes belonging to different ELL maps. Pharmacological experiments, immunohistochemistry and voltage clamp recordings are being carried out to determine the nature and dynamics of the conductances here proposed.

In contrast to other types of onset cells, spherical cells exhibit a long relative refractory period

We propose that the spherical cell's long refractory period could be caused by a slow deactivation of the low-threshold K^+ conductance. This hypothesis was tested by calculating the slope of *V/I* plots constructed at 1 ms after the onset of current steps, applied at different delays after a conditioning spike. The

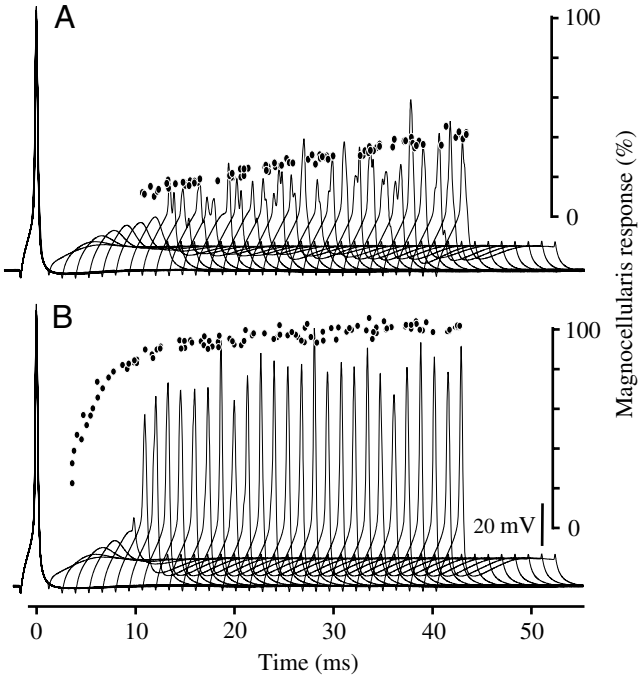

Fig. 11. The refractory period matches the duration of the low-responsiveness window. Averaged spherical cell responses obtained from 10 series of current test steps of constant intensity applied at different delays after a conditioning spike (traces) are superimposed on the amplitude of the magnocellularis nucleus responses to the conspecific-generated EOD shown in Fig. 2, normalized as a percentage of the amplitude of the self-generated EOD (black circles). (A) *In vitro* test step at 400 pA, conspecific located antiparallel at 6 cm; (B) *in vitro* test step 430 pA, conspecific located antiparallel at 3 cm. Resting membrane potential –70 mV, conditioning step 500 pA. In order to compare both graphs, zero magnocellularis response was aligned with the critical depolarization level and 100% magnocellularis response with the largest spike provoked by the self-generated EOD (right axis).

gradual increase of the *V/I* plot slope indicates that the membrane conductance gradually decays back to the resting value over 10–15 ms after the spike. Post-spike reduction in slope was well correlated with the increase in threshold and latency of the spikes generated by the same series of test steps, indicating that the refractory period of these neurons is due to an increase in membrane conductance rather than to inactivation of Na^+ channels. As the refractoriness is also elicited by subthreshold conditioning steps, the most parsimonious interpretation is that the same conductance that causes the outward rectification during the step also causes the refractoriness after the step.

As the long relative refractory period blocks the response to the second of a pair of afferent inputs, the described spherical cell's excitability implements the low-responsiveness window observed *in vivo* after the fast electrosensory pathway activation. The comparison made in Fig. 11 is based on the assumption that the temporal average of intracellular recordings from a single cell could mimic the summation of activities of similar cells recorded as a compound action potential.

Larger conspecific-generated EODs recruit more primary afferent fibers and, because of convergence, increase the probability of larger inputs on each cell, more easily overcoming the long lasting refractory period and, therefore, the low-responsiveness window (as shown in Fig. 2).

Afferent convergence and electrical synapses between neighboring spherical cells may also explain the graded decrease in responsiveness of the path as a whole with the increase in amplitude of the conditioning stimuli, as observed in Fig. 3. Increased conditioning stimuli result in a more complete recruitment of the afferent population. This causes refractoriness not only in the cells that fired to the conditioning afferent volley, but also in the fringe of those cells in which afferent input provoked subthreshold depolarizations (either directly or indirectly through a neighbor cell). Thus, increasing conditioning stimulus intensity reduces the responsiveness of the path.

Consequently, we propose that the self-generated EOD, a very strong stimulus repeated at intervals slightly longer than the low-responsiveness window that it generates, may permit the fish to maintain a continuous stream of self-generated information despite the occurrence of other potentially interfering electric signals as the conspecific-generated EODs. It is known that progressive incremental delays between self-generated EODs and conspecific-generated EODs cause transient increases in self-generated EOD rate (Bullock, 1969; Westby, 1975; Capurro et al., 1998). In fact, *G. carapo* discharges very regularly with a coefficient of variation of the inter-EOD interval less than 2%. By suddenly shortening the inter-EOD interval between 10 and 15% and returning slowly to the basal rate, fish provoke a phase shift between the self-generated and the conspecific EOD, which was interpreted (Westby, 1975) as a jamming avoidance response because the faster discharging fish appears to predict and avoid the joint occurrence of the conspecific-generated EOD and self-generated EOD. Our results indicate that jamming avoidance responses probably not only prevent an EOD collision, as previously thought, but are also the actual responses to increasing interference. In fact, as the delay increases between self-generated EOD and the EOD of a slower discharging conspecific, the delay between the conspecific-generated EOD and the next self-generated EOD decreases. This causes an increase of the number of spherical cells that leave the refractory period and respond to the conspecific-generated EOD. In turn, the increased recruitment of spherical cells by the conspecific-generated EOD decreases the number of spherical cells ready to be activated by the next self-generated EOD. Thus, as the delay between conspecific-generated EOD and the next self-generated EOD decreases, the response to this last one is more affected. This interference is maximal when the difference in frequency is small enough to interfere the response to several successive self-generated EODs. Fish respond to this interference with transient accelerations of the pacemaker that phase-reset the self-generated EOD in such a

way that the conspecific-generated EOD is forced to occur with a higher probability within the low-responsiveness window. As a result of the combination of the low-responsiveness window and the electromotor behavior, the response of the fast electrosensory pathway to the self-generated EOD is facilitated and the response to the interfering conspecific-generated EOD is stopped. Thus the sensory driven active control of the pacemaker rate may allow the fish to adjust the delay between self-generated EOD and conspecific-generated EOD in such a way that streaming of self-generated information is optimized.

Comparative considerations about single spiking cells

The presence of single spiking cells in sensory subsystems that are specialized for the preservation and analysis of timing information is not exclusive to the fast electrosensory pathway of pulse gymnotids. Neurons with similar characteristics and functional significance are present in the electrosensory systems of wave gymnotids (Szabo et al., 1975; Heiligenberg, 1991; Mehaffey et al., 2006), pulse (Bell and Grant, 1989; Xu-Friedman and Hopkins, 1999) and wave (Kawasaki, 2005) mormyrids, as well as in the auditory (Carr et al., 2005) and somatosensory (Prescott and De Koninck, 2002) systems of higher vertebrates.

The fast electrosensory pathway appears to be an electrosensory subsystem present in all fish exhibiting active electroreception (Szabo et al., 1975). The second order neurons of these paths are also round adendritic cells.

Although the fast electrosensory path in wave fish and in pulse mormyrids is very well described at the system and circuit levels, to our knowledge details of the intrinsic properties of the second order neurons remain still unexplored in most fish.

In gymnotids the characterization of spherical cell phenotype is incomplete. However, spherical cells appear to be adapted for implementing the information-processing task that the organization of the electromotor-electrosensory systems of each species imposes.

Eigenmannia spherical cells differ from those of *G. carapo* both in that they do not establish dendro-somatic connections and in that they project *via* the lateral lemniscus to the layer VI of the contralateral torus (Carr et al., 1981). As in pulse gymnotids, the EOD generates a synchronized activation of the fast electrosensory pathway of *Eigenmannia* (Szabo et al., 1975). To our knowledge, the functional properties of *Eigenmannia* ELL spherical cells are only mentioned in Heiligenberg's book (Heiligenberg, 1991) as following 1:1 a 170 Hz stimulus.

In *Apteronotus*, spherical cells project onto a mesencephalic magnocellularis nucleus (unique and medial as in pulse gymnotids) firing one to one with the EOD at about 1 kHz (Szabo et al., 1975). While jamming avoidance responses consist of long-lasting changes of the pacemaker rate in wave fish, pulse fish frequently exhibit transient accelerations (Bullock, 1969). This implies differences in both signal processing and intrinsic properties of spherical cells. In fact, a long refractory period of spherical neurons would be inadequate for reafferent signal processing in high frequency wave fish. This conjecture agrees with the immunohistochemical finding of high threshold K^+ channels in spherical cells of *Apteronotus* (Mehaffey, 2006) that may facilitate spike repolarization and reduce the refractory period, as shown for other cell types in the electrosensory lobe of *Apteronotus* (Rashid, 2001; Fernandez et al., 2005).

Single spiking cells with similar outward and inward rectification were also described in the dorsal horn of mammals (Prescott and De Koninck, 2002) but their functional role in the computation of somatosensory images appears to be still obscure (Graham et al., 2004).

Finally, the spherical cells of pulse fish have much in common with auditory cells of birds and mammals (Carr, 2004). The combination of conductances described is similar to that exhibited by bushy and octopus cells in mammalian ventral cochlear nucleus (Golding et al., 1999; Manis and Marx, 1991; Wu and Oertel, 1984; Brew and Forsythe, 1995; Oertel et al., 2000), and avian angularis, magnocellularis and lemniscal nucleus, which share with spherical cells the accurate transmission of information using a latency code (Trussell, 1999; Rathouz and Trussell, 1998; Reyes et al., 1994; Soares et al., 2002).

These comparative data suggest that single spiking cells and their intrinsic properties are a convergent solution in the evolution of sensory systems (Carr, 2004; Carr et al., 2005). However, species variations may adapt cell structure and specific functions reciprocally. The K^+ low-threshold conductance described for pulse fish spherical cell deactivates slowly, as does the low-threshold K^+ channel observed in auditory cells of guinea pig (time constant 12.5 ms) (Manis and Marx, 1991). This K^+ conductance appears to be the same that shapes octopus cell responsiveness in mice (Golding et al., 1999). In other auditory cells, low-threshold K^+ conductance is supplemented by the presence of a high-threshold K^+ conductance (Carr et al., 2005). As in the pyramidal cells of the ELL of *Apteronotus*, the high-threshold conductance facilitates spike repolarization and accelerates deactivation of the low-threshold current, allowing the auditory onset cells to follow high frequency stimuli (Manis and Marx, 1991; Trussell, 1999).

This work was entirely performed in the Department of Integrative and Computational Neurosciences, Instituto de Investigaciones Biológicas Clemente Estable. J.N. and M.E.C. are also members of the Department of Histology and Embryology of the Faculty of Medicine, which covered part of the salary of J.N. and M.E.C. J.N. performed *in vitro* experiments, participated in their data analysis and manuscript correction. M.E.C. performed *in vivo* experiments, participated in their data analysis and manuscript correction. A.A.C. conceived the study and experimental designs, participated in both types of experiments, their data analysis and wrote the first draft of the manuscript. We thank to Drs C. C. Bell, M. Borde and J. C. Velluti for their thoughtful and helpful comments on the manuscript. It was partially supported by Fogarty #1R03-TW05680, Fondos Clemente

Estable #4014 and 9036 ECOS-Sud project #U03B01 and PEDECIBA.

References

Aguilera, P. A., Castelló, M. E. and Caputi, A. A. (2001). Electroreception in *Gymnotus carapo*: differences between self-generated and conspecific-generated signal carriers. *J. Exp. Biol.* **204**, 185-198.

Albert, J. and Crampton, W. G. R. (2005). Diversity and phylogeny of neotropical electric fishes (Gymnotiformes). In *Electroreception*, vol. 21 (ed. T. H. Bullock, C. D. Hopkins, A. N. Popper and R. R. Fay), pp. 360-409. New York: Springer.

Arbib, M. A., Erdi, P. and Szentagothai, J. (1997). *Neural Organization: Structure, Function, and Dynamics.* Cambridge (MA): MIT Press.

Bal, R. and Oertel, D. (2000). Hyperpolarization-activated, mixed-cation current (I (h)) in octopus cells of the mammalian cochlear nucleus. *J. Neurophysiol.* **84**, 806-817.

Bell, C. C. and Grant, K. (1989). Corollary discharge inhibition and preservation of temporal information in a sensory nucleus of mormyrid electric fish. *J. Neurosci.* **9**, 1029-1044.

Black Cleworth, P. (1969). Social behavior in *Gymnotus carapo* (Pisces; Gymnotidae). PhD thesis, University of California, Los Angeles, USA.

Brew, H. M. and Forsythe, I. D. (1995). Two voltage-dependent K^+ conductances with complementary functions in postsynaptic integration at a central auditory synapse. *J. Neurosci.* **15**, 8011-8022.

Bullock, T. H. (1969). Species differences in effect of electroreceptor input on electric organ pacemakers and other aspects of behavior in electric fish. *Brain Behav. Evol.* **2**, 85-118.

Bullock, T. H., Hagiwara, S., Kusano, K. and Negishi, K. (1961). Evidence for a category of electroreceptors in the lateral line of gymnotid fishes. *Science* **134**, 1426-1427.

Capurro, A., Macadar, O., Perrone, R. and Pakdaman, K. (1998). Computational model of the jamming avoidance response in the electric fish *Gymnotus carapo*. *Biosystems* **48**, 21-27.

Carr, C. E. (2004). Timing is everything: organization of timing circuits in auditory and electrical sensory systems. *J. Comp. Neurol.* **472**, 131-133.

Carr, C. E., Maler, L., Heiligenberg, W. and Sas, E. (1981). Laminar organization of the afferent and efferent systems of the torus semicircularis of gymnotiform fish: morphological substrates for parallel processing in the electrosensory system. *J. Comp. Neurol.* **203**, 649-670.

Carr, C., Iyer, S., Soares, D., Caluri, S. and Simon, J. Z. (2005). How neurons compute: examples from temporal coding. In *23 Problems in Systems Neuroscience* (ed. J. L. van Hemmen and T. J. Sejnowski), pp. 245-265. Oxford: Oxford University Press.

Castelló, M. E., Caputi, A. and Trujillo-Cenóz, O. (1998). Structural and functional aspects of the fast electrosensory pathway in the electrosensory lateral line lobe of the pulse fish *Gymnotus carapo. J. Comp. Neurol.* **401**, 549-563.

Fernandez, F. R., Mehaffey, W. H., Molineux, M. L. and Turner, R. W. (2005). High-threshold K^+ current increases gain by offsetting a frequency-dependent increase in low-threshold K^+ current. *J. Neurosci.* **25**, 363-371.

Golding, N. L., Ferragamo, M. J. and Oertel, D. (1999). Role of intrinsic conductances underlying responses to transients in octopus cells of the cochlear nucleus. *J. Neurosci.* **19**, 2897-2905.

Graham, B. A., Brichta, A. M. and Callister, R. J. (2004). In vivo responses of mouse superficial dorsal horn neurones to both current injection and peripheral cutaneous stimulation. *J. Physiol. (Lond.)* **561**, 749-763.

Heiligenberg, W. (1991). *Neural Nets in Electric Fish.* Cambridge (MA): MIT Press.

Horikawa, K. and Armstrong, W. E. (1988). A versatile means of intracellular labeling: injection of biocytin and its detection with avidin conjugates. *J. Neurosci. Methods* **25**, 1-11.

Kawasaki, M. (2005). Physiology of tuberous electrosensory systems. In *Electroreception,* vol. 21 (ed. T. H. Bullock, C. D. Hopkins, A. N. Popper and R. R. Fay), pp. 154-194. New York: Springer.

Koch, C. and Segev, I. (2000). The role of single neurons in information processing. *Nat. Neurosci.* **3**, 1171-1177.

Lissmann, H. W. (1951). Continuous electrical signals from the tail of a fish. *Gymnarchus niloticus* Cuv. *Nature* **167**, 201-202.

Lissmann, H. W. (1958). On the function and evolution of electric organ in fish. *J. Exp. Biol.* **35**, 156-191.

Llinas, R. R. (1988). The intrinsic electrophysiological properties of mammalian neurons: insights into central nervous system function. *Science* **242**, 1654-1664.

Manis, P. B. and Marx, S. O. (1991). Outward currents in isolated ventral cochlear nucleus neurons. *J. Neurosci.* **11**, 2865-2880.

Marder, E. (2002). Non-mammalian models for studying neural development and function. *Nature* **417**, 318-321.

Marr, D. (1982). *Vision.* New York: Freeman.

Mehaffey, W. H., Fernandez, F. R., Rashid, A. J., Dunn, R. J. and Turner, R. W. (2006). Distribution and function of potassium channels in the electrosensory lateral line lobe of weakly electric apteronotid fish. *J. Comp. Physiol. A* doi: 10.1007/s00359-006-0103-z.

Oertel, D., Bal, R., Gardner, S. M., Smith, P. H. and Joris, P. X. (2000). Detection of synchrony in the activity of auditory nerve fibers by octopus cells of the mammalian cochlear nucleus. *Proc. Natl. Acad. Sci. USA* **97**, 11773-11779.

Pereira, A. C., Centurion, V. and Caputi, A. A. (2005). Contextual effects of small environments on the electric images of objects and their brain evoked responses in weakly electric fish. *J. Exp. Biol.* **208**, 961-972.

Prescott, S. A. and De Koninck, Y. (2002). Four cell types with distinctive membrane properties and morphologies in lamina I of the spinal dorsal horn of the adult rat. *J. Physiol.* **539**, 817-836.

Rashid, A. J., Morales, E., Turner, R. W. and Dunn, R. J. (2001). The contribution of dendritic Kv3 K^+ channels to burst discharge in a sensory neuron. *J. Neurosci.* **21**, 125-135.

Rathouz, M. and Trussell, L. (1998). Characterization of outward currents in neurons of the avian nucleus magnocellularis. *J. Neurophysiol.* **80**, 2824-2835.

Réthelyi, M. and Szabo, T. (1973). Neurohistological analysis of the lateral lobe in a weakly electric fish, *Gymnotus carapo* (Gymnotidae, Pisces). *Exp. Brain Res.* **18**, 323-339.

Reyes, A., Rubel, E. and Spain, W. (1994). Membrane properties underlying the firing of neurons in the avian cochlear nucleus. *J. Neurosci.* **14**, 5352-5364.

Schlegel, P. A. (1973). Perception of objects in weakly electric fish *Gymnotus carapo* as studied in recordings from rhombencephalic neurons. *Exp. Brain Res.* **18**, 340-354.

Soares, D., Chitwood, R. A., Hyson, R. L. and Carr, C. E. (2002). Intrinsic neuronal properties of the chick nucleus angularis. *J. Neurophysiol.* **88**, 152-162.

Szabo, T., Sakata, H. and Ravaille, M. (1975). An electrotonically coupled pathway in the central nervous system of some teleost fish, Gymnotidae and Mormyridae. *Brain Res.* **95**, 459-474.

Trussell, L. O. (1999). Synaptic mechanisms for coding timing in auditory neurons. *Annu. Rev. Physiol.* **61**, 477-496.

Westby, G. W. (1979). Electrical communication and jamming avoidance between resting *Gymnotus carapo. Behav. Ecol. Sociobiol.* **4**, 381-393.

Westby, G. W. M. (1975). Has the latency dependent response of *Gymnotus carapo* to discharge triggered stimuli a bearing in electric fish communication? *J. Comp. Physiol. A* **96**, 307-341.

Wu, S. H. and Oertel, D. (1984). Intracellular injection with horseradish peroxidase of physiologically characterized stellate and bushy cells in slices of mouse anteroventral cochlear nucleus. *J. Neurosci.* **4**, 1577-1588.

Xu-Friedman, M. A. and Hopkins, C. D. (1999). Central mechanisms of temporal analysis in the knollenorgan pathway of mormyrid electric fish. *J. Exp. Biol.* **202**, 1311-1318.